

# On Joint Design with Intrinsic Variable Compliance: Derivation of the DLR QA-Joint

Oliver Eiberger, Sami Haddadin, Michael Weis, and Alin Albu-Schäffer & Gerd Hirzinger

**Abstract**—In this paper we introduce a classification of intrinsically compliant joint mechanisms. Furthermore, we outline design considerations for realizing such devices in order to match the requirements for robust and performant actuation. Based on this elaboration, a new design concept is presented, the DLR QA-Joint. Its performance is investigated by various experiments, covering velocity increase using the elastic energy, joint protection capabilities, and control performance.

## I. INTRODUCTION

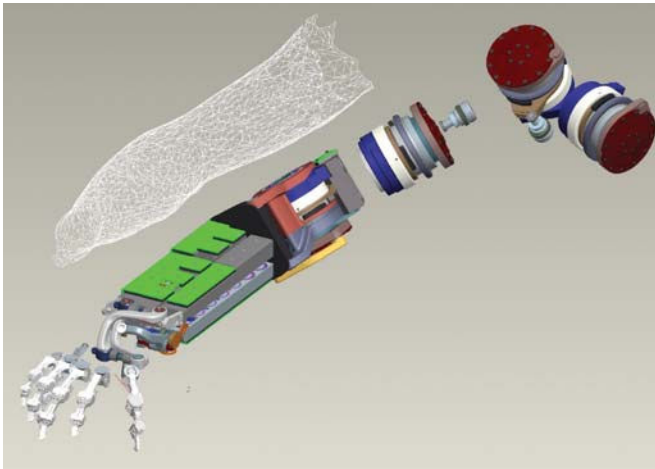


Fig. 1. The DLR hand-arm system.

Human-friendly robotics is one of the major challenges of nowadays robotics, which led to new robot designs especially well suited for coping with the uncertainties of unknown and unstructured environments [1], [2], [3], [4]. These robots are usually characterized either by active compliance control or intrinsically compliant behavior. Active compliance control has reached already a very mature stage and recently went to market: the KUKA Lightweight Robot, which was developed at DLR, and whose technology has been transferred to the robot manufacturer KUKA, is a fully joint-torque controlled lightweight robot providing various soft-robotics control features. Intrinsic compliance on the other hand is currently investigated in several large European and worldwide research projects. Due to the significant increase in mechanical design complexity, the additional degrees of freedom and related questions regarding control, there are still several open issues to be addressed. At DLR we currently develop an integrated hand-arm system [5], [6], which will be fully equipped with variable stiffness actuation, c.f. Fig.1.

E. Eiberger, S. Haddadin, A. Albu-Schäffer, and Gerd Hirzinger are with Institute of Robotics and Mechatronics, DLR - German Aerospace Center, Wessling, Germany [oliver.eiberger@dlr.de](mailto:oliver.eiberger@dlr.de), [sami.haddadin@dlr.de](mailto:sami.haddadin@dlr.de), [alin.albu-schaeffer@dlr.de](mailto:alin.albu-schaeffer@dlr.de)

In this paper we present general design considerations for intrinsically compliant joints, leading to a new design concept, the Quasi-Antagonistic Joint (QA-Joint). The presented approach has an elastically coupled drive unit with variable stiffness that is achieved via superposition of antagonistic torque/displacement characteristics. Furthermore, we investigate velocity gain and joint protection capabilities due to the inherent elastic behavior of such mechanisms in detail, and support the results by numerous experiments.

The paper is organized as follows. Section II introduces a new classification attempt for intrinsically compliant joint designs and gives an overview of already existing ones. Section III introduces our design considerations for realizing these novel mechanisms, leading to the prototype presented in Sec. IV. The identification of stiffness and friction is shown in Sec.V, while the achievable results in velocity increase are outlined in Sec.VI. Finally Sec.VII proves the performance in joint protection during highly dynamic impacts and Sec.VIII concludes the paper.

## II. INTRINSICALLY COMPLIANT ACTUATION

Since the early 1980's, different approaches were made to realize compliant joint coupling. The motivation originated mainly from using inherent elasticity to achieve stable behavior during hard contact, protecting the joints from impact shock, and storing elastic energy e.g. for energy efficient motions.

In an intrinsically compliant joint mechanism the relation between the elastic force  $F_E \in \mathbb{R}$ , acting along the generalized displacement coordinate  $x_E \in \mathbb{R}$  in the axis of the compliant element, to the elastic joint torque  $\tau_J \in \mathbb{R}$  can be written as a possibly nonlinear transformation

$$\tau_J = \int_{x_0}^{x_1} \underbrace{\frac{\partial F_E}{\partial x_E}}_{K_{x_E}} dx_E \frac{\partial x_E}{\partial \varphi}, \quad (1)$$

where  $\partial F_E / \partial x_E$  is the generalized stiffness and  $\partial x_E / \partial \varphi$  the transmission rate. (1) holds for all four combinations of linear and nonlinear stiffness and transmission rate. In this paper we treat only linear stiffness elements, which are producing nonlinear output behavior via a nonlinear transmission<sup>1</sup>. A selection of designs is shown in Tab. I. Despite their very different technical realizations, we believe they can be grouped into two main branches of development.

- 1) Preload variable design
- 2) Transmission variable design

In the following we describe the unifying characteristics, which justify the proposed classification.

<sup>1</sup> $K_{x_J}$  denotes from now on only constant stiffness so the stored elastic energy can be simply described as  $E_J = E_E = \frac{1}{2} K_{x_E} x_E^2$ .

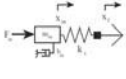
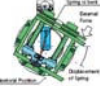

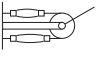
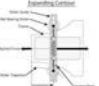
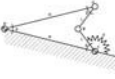
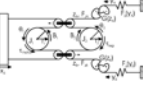
Example	SEA[7]	MIA[8]	MACCEPA[9], DLR VS-Joint[13]	McKibben[10]	GATECH[11]	VSA[3], VSA-II[14]	AMASC[12], DLR QA-Joint
Setup	Serial Spring	Serial tunable spring	Symmetric spring, progressive trans.	Antagonistic	Antagonistic	Antagonistic Push-Pull	Quasi-Antagonistic
Stiffness variation	Constant	Constant	Progressive	Progressive	Progressive	Progressive	Progressive
Adjustable	No	Yes	Yes	Yes	Yes	Yes	Yes
Characteristics variation	No	Spring constant	Preload	Preload	Superposition	Superposition/Double	Superposition
Stiffness actuator	No	Yes	Yes	No	No	No	Yes
Picture							

TABLE I  
CLASSIFICATION OF JOINT ARCHITECTURES

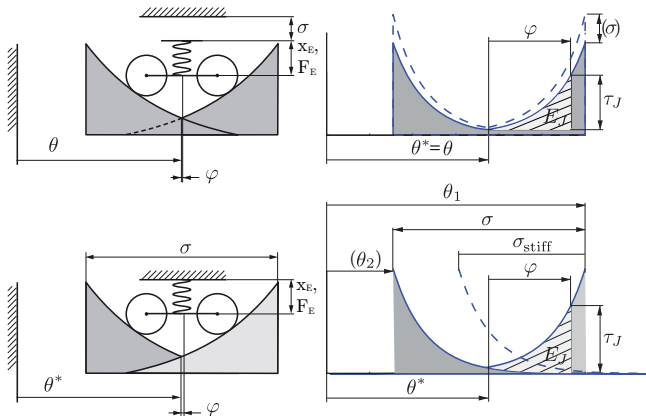


Fig. 2. Preload variable type (upper row). Transmission variable type (lower row). The left plots depict the mechanical transmission and the right ones the torque displacement.

a) *Preload variable design*: In Figure 2 (upper row), the *preload variable type* is depicted.  $\sigma$  denotes the pre-compression of the elastic element and  $x_E$  is directly associated with it. The mechanism is characterized by the fact that one actuator, with coordinate  $\theta$ , is moving the entire elastic mechanism and therefore, the equilibrium point  $\theta^* = \theta$ . The elastic deflection is  $\varphi = \theta - q$  and the elastic joint torque can be described as

$$\tau_J = K_{x_E}(x_E(\sigma) + x_E(\varphi)) \frac{\partial x_E(\varphi)}{\partial \varphi}. \quad (2)$$

Important to notice is the fact that the elastic force depends for a constant  $\sigma$  only on the deflection  $\varphi$  with an offset force generated through  $\sigma$ . Furthermore, the transmission is only a function of  $\varphi$ . For the preload variable design the choice of actuator variables is unambiguously  $\theta$  and  $\sigma$ .

b) *Transmission variable design*: For the transmission variable type the main difference compared to the preload variable design is that four possible choices of actuation variables exist (two out of  $\theta_1, \theta_2, \sigma$  or all three). This is due to the fact that for these designs the transmission element for each direction can possibly be moved independently from the other.  $\theta_1, \theta_2, \theta^* \in \mathbb{R}$  are the absolute positions of the curves in world coordinates and the equilibrium position.  $\sigma \in \mathbb{R}$  is the displacement between the curves and  $\varphi \in \mathbb{R}$  the deflection. For antagonistic systems the pair of choice is  $(\theta_1, \theta_2)$  and in the QA-Joint  $(\theta_1, \sigma)$  presented later are chosen. As depicted in Fig. 2 (lower), we can write the

kinematic relations as

$$\sigma = \theta_2 - \theta_1 \quad (3)$$

$$\theta^* = \theta_1 + \frac{1}{2}\sigma = \frac{\theta_1 + \theta_2}{2} \quad (4)$$

$$\varphi = \theta^* - q. \quad (5)$$

This leads to the elastic joint torque

$$\tau_J = K_{x_E} x_E \left( \varphi + \frac{\sigma}{2} \right) \frac{\partial x_E(\varphi + \frac{\sigma}{2})}{\partial \varphi}. \quad (6)$$

In contrast to the *preload type*, the elastic force of the *transmission type* depends on  $\varphi + \frac{\sigma}{2}$ , as well as the transmission does. This leads e.g. for an exponential progression type to a change in the exponent, thus to a high variation in stiffness.

The *preload variable* branch evolved from constant stiffness towards symmetrically acting progressive stiffness assemblies. Thus, it represents a technical approach towards an integrated mechanism with limited complexity. The *transmission variable* group showcases the development from human like antagonistic actuation towards related actuation mechanisms that use superposition of torque/displacement characteristics for stiffness variation. Simultaneously, they intend to overcome the drawbacks of equally sized drives for opposing directions. On the one hand, the number of parts and expected complexity of this line of developments appears to be larger. On the other hand, the superposition of individual characteristics allows for new ways to influence the overall behavior of the mechanism.

### III. DESIGN CONSIDERATIONS

The human has the ability to co-contract his muscles to react with appropriate stiffness to perturbations and relax them almost instantaneously to become fully backdriveable. This is e.g. especially useful during high-performance tasks as throwing a ball or evading from external forces to prevent muscle damage due to overload. To mimic such capabilities in a technical system requires series elastic coupling with variable impedance and high backdriveability. Current systems hardly fulfill all requirements at the same time and are clearly outperformed by human actuation e.g. by means of load-to-weight ratio, payload, and speed capabilities. In this sense we discuss the following general requirements, which we believe to be important in order to come closer to human-like actuation performance. We elaborate a joint design space, taking into account external influences as well as internal relations of different design aspects.

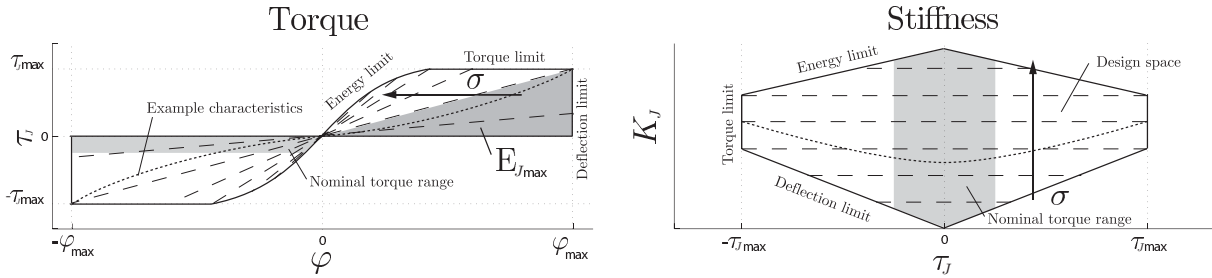


Fig. 3. Design space for torque displacement curves (left). Stiffness over torque (right).

### A. Joint design aspects

The most important properties of a robot joint are

- Maximum (stall) joint torque  $\tau_{J,\max}$ .
- Maximum (static) joint speed  $\dot{\theta}_{\max}$ .

In contrast to a stiff robot, additional design aspects have to be considered for intrinsically compliant mechanisms:

- Joint elastic deflection range  $\varphi$ : free motion vs. mechanical limits.
- Joint stiffness range  $K_J$ : appropriate shape and limits.
- Energy storage capacity  $E_J$ : for energy absorption and dynamic tasks.

For a passively elastic robot joint, its characteristics can generally be visualized by two specific graphs. The torque-deflection (Fig. 3 (left)) and stiffness-torque (Fig. 3 (right)) plots are suitable for determining desired properties of a compliant mechanism.

In Figure 3 (upper), limits due to maximum joint torque, maximum elastic deflection, and maximum potential energy span an elastic design space, in which the characteristics of the centering torque  $\tau_J$  over passive deflection  $\varphi$  can be plotted (see also Fig. 6). Stored potential energy through deflection is visualized as the area below a torque deflection curve. If we consider the case of adjustable linear joint stiffness (dashed lines) with constant maximum deflection  $\forall \sigma$  as the ideal joint, the aforementioned constraints limit the practically achievable design. Due to mechanical torque limits there exists a maximum  $\tau_{J,\max}$ . Therefore the maximum deflection  $\varphi_{\max}$  is a function of  $\sigma$ . This induces a second problem. If we choose linear spring behavior, the maximum joint torque will be a function of  $\sigma$ , leading to higher strike through risk for very low stiffness. This is due to low energy storage and low maximum torque at the same time. The *energy limit* is mainly caused by limited deflection  $x_{E,\max}$  of physical springs. Consequently, the amount of energy required for stiffening the joint by internal tension is not accessible anymore for further elastic deflection.

The second characteristic graph, depicted in Figure 3 (lower), plots the stiffness characteristics  $K_J$  of the elastic element with respect to joint torque in the same design space limits. In particular, this plot intuitively visualizes the achievable stiffness under a given load. Again, we consider it to be desirable to achieve variable constant stiffness (dashed lines), especially in the so called *nominal torque range*.

In the following some essential aspects regarding the above mentioned properties are addressed.

- *Joint torque*. It is from our perspective desirable for an elastic joint mechanism to maintain the torque capacity for the entire stiffness preset range as good as possible. Most elastic mechanisms show decreasing torque

capacity in stiff operation mode, due to internal spring preload.

- *Elastic motion range*. Since robots have a limited motion range, the maximum elastic deflection of the joints needs to be considered. The maximum joint torque required to prevent strike through must always be attainable before the mechanical limit, either by limiting  $\theta$  to  $q_{\max} - \varphi_{\max}$  and/or through active reaction schemes. In relation to the expected motion range and considering the range extension obtainable by reactive motion, a maximum elastic deflection of  $15^\circ$  seems appropriate for humanoid arm joints.
- *Joint stiffness*. The predominant external load is expected to be within  $\approx 25\%$  of the maximum joint torque  $\tau_{J,\max}$ , when assuming general manipulation tasks under gravity influence without major accelerations. In this nominal torque range it is especially desired to be able to alter the joint stiffness in a wide range to cover differing stiffness demands. Since the external load may vary as a result of pose changes as well as due to reaction forces during contact, it is desirable to maintain constant stiffness behavior under varying load, easing manipulation tasks and simplifying control schemes.
- *Minimum stiffness*. In case of obtaining joint torque information by measuring deflection, zero joint stiffness is not considered as desirable, because torque information is lost, as does controllability of the joint. In particular, it might not be restored quickly enough to ensure short reaction times.
- *Maximum stiffness*. Since one the major purposes of elastic joints is robot and environment protection, limiting the maximum stiffness is an important issue. The maximum stiffness significantly defines the chance for reaction in case of an impact. Thus, it influences the available load capacity for heavy manipulation tasks, demanding safety reserves in deflection to sustain collisions. A relative collision, leading to  $\dot{q}_c = \dot{\theta}_{\max}$ , where  $\dot{\theta}_{\max}$  is the maximum motor velocity, relates to the worst case time  $t_{cr}$  needed to react as

$$t_{cr} = t_{cd} + \frac{B\dot{\theta}_{\max}}{\tau_m}, \quad (7)$$

where  $t_{cr}, t_{cd}$  are the collision reaction and collision detection time, while  $B$  and  $\tau_m$  are the motor inertia and motor torque. A purely geometric minimum deflection reserve is obtained.

$$\varphi_{\text{res}} = t_c \dot{\theta}_{\max}. \quad (8)$$

Characteristics	$\frac{1}{\varphi}$	$e^\varphi$	$\varphi^2$
Constant stiffness	-	+	++
Minimum stiffness	--	-	+
Maximum stiffness	++	+	--
Spring Energy	-	+	++
Joint protection	$\pm$	+	-

TABLE II  
COMPARISON OF TORQUE CHARACTERISTICS

To be able to utilize most of the joint maximum torque (e.g.  $1-c = 95\%$ ), maximum stiffness has to be limited to

$$\int_{\sigma-\varphi_{\text{res}}}^{\sigma} K(\sigma, \varphi) d\varphi \leq c\tau_{J,\text{max}}. \quad (9)$$

These conditions determine the relationship between applicable load with safe speed and stiffness.

- **Energy storage.** The potential joint elasticity can be used for absorbing kinetic energy of an impact or during catching heavy objects. It can also be used for additional acceleration of the link [13], [15] by appropriate motion. However, one has to be aware that the stored energy may also cause unwanted acceleration. This is e.g. the case when losing contact to an object or due to malfunction. Thus, the energy level should be kept moderate and the reaction of the active parts has to be fast enough to prevent severe damage in case of faults.

The properties described above influence the choice of the torque displacement characteristics significantly. Unfortunately, they cannot be maximized at the same time. In Table II we qualify the influence of selected torque/deflection characteristics, comparing rational, low progressive exponential, and quadratic torque displacement curves.

#### IV. JOINT DESIGN AND MODEL

For the technical realization of the joint it is important to achieve a compact design and light-weight structure for low inertia and thus high bandwidth of the robot. Furthermore, it is crucial for most control features developed at DLR to provide high quality torque feedback, which implies low friction and low hysteresis in the compliant mechanism.

##### A. Joint design

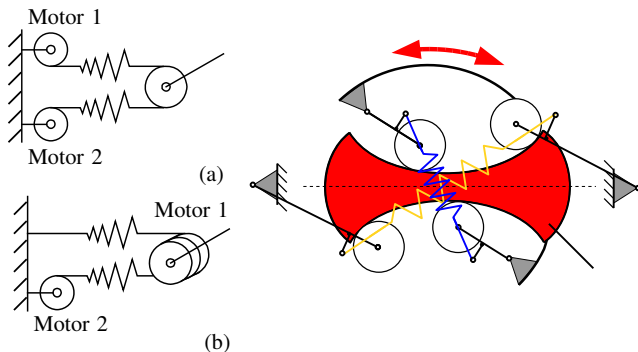


Fig. 4. Variable Stiffness Actuator with nonlinear progressive springs in antagonistic (a) and quasi antagonistic (b) realization. Principle of the elastic mechanism (right).

Overall, the superposition of agonist and antagonist action with different offsets results in the desired variable stiffness. The QA-Joint consists of a link positioning drive with HarmonicDrive gears and the elastic mechanism with the

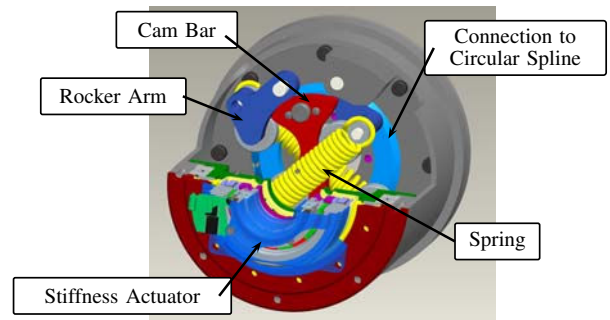


Fig. 5. Cross section of the Quasi Antagonistic Joint design.

Property	Value
Torque capacity	$\tau_{J,\text{max}} = 40 \text{ Nm}$
Maximum positioning drive speed	$\dot{\theta}_{\text{max}} = 3.8 \text{ rad/s}$
Maximum elastic deflection	$\varphi_{\text{max}} = 3 \dots 15^\circ$
Maximum spring energy	$E_\varphi^{\text{max}} = 2 \times 2.7 \text{ J}$
Stiffness range ( $\tau_J = 0$ )	$20 \dots 750 \text{ Nm/rad}$
Maximum stiffness adjustment time	0.12 s
Mass	1.2 kg

TABLE III  
TESTBED PROPERTIES

stiffness actuation drive. The main difference to a classical antagonistic joint is that the two motors are not used in a symmetric configuration as agonist and antagonist, c.f. Fig. 4 a. Instead, one motor (the link drive) adjusts the link side position, while the second motor (the stiffness drive) operates stiffness adjustment, c.f. Fig. 4 b. With this arrangement the adjustment of position and stiffness are already decoupled to a high extend in hardware design. This special form of antagonistic actuation is very advantageous for configurations with pronounced agonist actuation.

The compliance consists of two progressive elastic elements opposing each other with a variable offset that supports the link with variable range of elastic motion, c.f. Fig. 5. The ordinary fixed Circular Spline of the Harmonic Drive gear for link positioning is held in a bearing and has a cam bar attached to it. Two pairs of rocker arms with cam rollers, each pair linked by a linear spring, act on different faces of this cam bar. External loads result in rotational displacement of the entire gear and force the rocker arms of the supporting direction to spread against the linear spring. This causes a progressive centering torque. The agonist rocker arms are fixed w.r.t. the housing. The opposing antagonist part is positioned with a rotational offset w.r.t. the stiffness actuator. This makes it possible to change stiffness independently from link speed in  $\approx 120 \text{ ms}$  for full stiffness range. In the QA-Joint the link position can be changed without moving the elasticity mechanism. This significantly reduces the inertia of the moving part of the joint.

The use of a cam-roller mechanism offers another advantage: The shape of the cam faces can be adapted to provide any desired torque characteristic that fits the maximum potential energy storable in the linear spring. Thus, the design is well suited to realize different torque/displacement characteristics with little overhead. In Table III the characteristics of the realized prototype are listed.

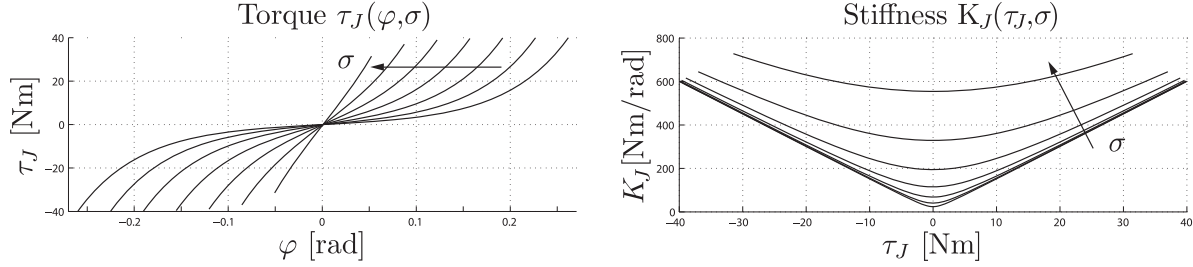


Fig. 6. Centering elastic joint torque over displacement curves for different stiffness presets (left). Stiffness values over elastic joint torque (right).

### B. Torque characteristics layout

For the shape of the torque/displacement curve an exponential characteristic is considered to be well suited, see also Tab. II. This is due to the fact that it results in a set of relatively constant stiffness curves over a wide load range, while providing large stiffness adjustment ranges. It allows moderate progression towards the elastic limits to protect the joint from strike through. Furthermore, the mathematical simplicity is obvious. The exponential stiffness has the general form

$$\tau_J = ae^{b((\theta-q)-\sigma)}, \quad (10)$$

where  $\sigma \in \mathfrak{R}$  denotes the displacement of the stiffness preset actuator. It is also an upper limit for the elastic deflection  $\varphi := (\theta - q) \in \mathfrak{R}$ , which can be obtained for a given preset.

$$(\theta - q) \leq \sigma \quad (11)$$

The design coefficients  $a, b \in \mathfrak{R}$  set the maximum torque and the elastic joint characteristic. They are chosen to be  $a = 40.0 \text{ Nm}$  and  $b = 15.0 \text{ rad}^{-1}$ . Therefore, the joint torque becomes

$$\tau_J = 40e^{15(\varphi-\sigma)} \quad (12)$$

for the implemented design.  $a$  denotes the torque at which the stored energy equals the maximum potential energy of the springs. For the full design of the hand-arm system (c.f. Fig. 1) it is planned to use the even less progressive exponential characteristics  $e^{12(\theta-q)}$  for each joint in the arm. Thus,  $a$  is varied according to the desired maximum torque value and the available spring energy. The geometry of the joint, in particular of the cam-roller mechanism, is derived from this target torque curve. The superposition of the two opposing elastic elements results for the complete joint model in a centering torque

$$\tau_J = 40(e^{15(\varphi-\sigma)} - e^{15(-\varphi-\sigma)}), \quad (13)$$

leading to the torque/deflection curves shown in Fig. 6 (left).

The corresponding stiffness adjustment range is shown in Fig. 6 (right). It is easily visible, that changing  $\tau_J$  results only in moderate stiffness change until deflection comes close to the end of the elastic range. In the nominal torque area, stiffness can be varied from below  $100 \text{ Nm/rad}$  to more than  $550 \text{ Nm/rad}$ .

### C. Model of the QA-Joint

The model of the QA-Joint incorporates the full motor dynamics, the elastic nonlinear joint torque and the link side

inertia. Furthermore, we take into account the friction and gravity torque.

$$B\ddot{\theta} = \tau_m - \tau_J \quad (14)$$

$$M\ddot{q} = \tau_J - \tau_F - \tau_g - \tau_{\text{ext}} \quad (15)$$

$B, M \in \mathfrak{R}$  are the motor and link side inertia, respectively.  $\theta, q \in \mathfrak{R}$  are the motor and link side position, and  $\tau_m, \tau_J, \tau_F, \tau_g, \tau_{\text{ext}} \in \mathfrak{R}$  the motor, elastic, friction, gravity, and external torque. Please note that we assume the stiffness actuator dynamics to be without significant dynamic influence on the joint drive and the link, c.f. Fig. 7. As will be shown in Sec. V, the major influences on the friction torque are the elastic deflection, load, and stiffness preset of the joint. For the motor we consider the maximum torque to be limited. Furthermore, the motor is controlled with simple PD control for the identification phase.

The structure of the nonlinear system is depicted in Fig. 7. Please note that the friction torque is modeled as pure Coulomb friction, depending on  $\text{sgn}(\dot{\varphi})$ .

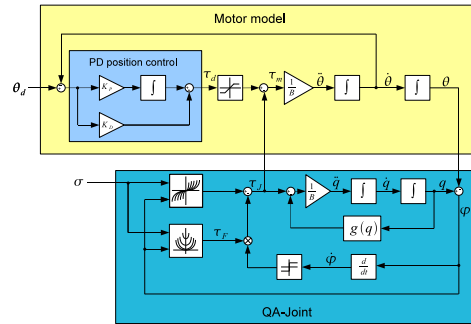


Fig. 7. Block diagram of the QA-Joint

## V. JOINT IDENTIFICATION

In order to generate the data for identifying the real elastic behavior and friction, the link is clamped and the position motor drives with different velocities at various stiffness presents within the elastic joint limits, c.f. Fig. 8 (left). The used sensors for identification are motor position sensors for  $\theta_1, \sigma, q$  and a link side joint torque sensor. The resulting measurements for friction and characteristics identification, together with the ideal model of the joint are given in Fig. 8 (right) and Fig. 9 for cyclic rectangular motions with  $\theta_d \in \{30 \ 60 \ 90\} \text{ }^\circ/\text{s}$ . The real behavior is characterized by a hysteresis and significant deviation from the ideal one<sup>2</sup>.

<sup>2</sup>Please note that for all experiments except the control performance in Sec. VII we use only simple motor side PD control in order to fully exploit the intrinsic capabilities of the joint.

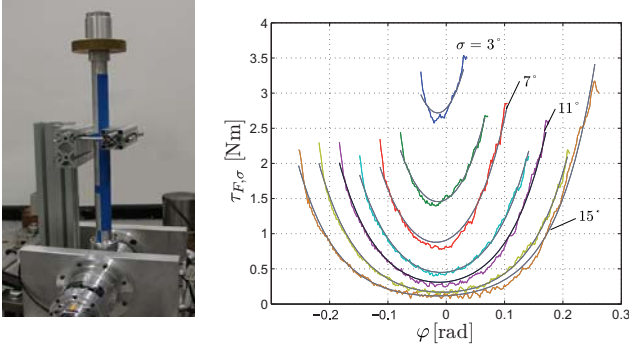


Fig. 8. QA-Joint with clamped link (left). Experimental friction torque over elastic deflection compared with the model friction (right). The corresponding values for  $\sigma$  are given in Tab. IV.

$\sigma$	$a_S$ [Nm]	$b_S$ [Nm]	$a_F$ [Nm]	$b_F$ [Nm]
$3^\circ$	26.2760	26.2221	2.5172	3.8480
$5^\circ$	26.6049	27.1703	2.6125	3.2755
$7^\circ$	26.8106	27.8989	2.9776	3.1582
$9^\circ$	26.4714	28.4042	2.3106	3.0784
$11^\circ$	26.3446	28.6174	2.8776	3.3393
$13^\circ$	26.0417	29.1079	2.4160	3.3339
$15^\circ$	22.7286	30.1821	3.3058	3.3004

TABLE IV  
IDENTIFIED COMPLIANCE AND FRICTION COEFFICIENTS

The real stiffness characteristics  $\tau_J^* \in \mathfrak{R}$  are estimated from the measurements. They are assumed to be the center lines of the hysteresis and are calculated as the arithmetic mean of the measured hysteresis. For the identification the following model is used, setting the coefficients of the exponential function free.

$$\tau_J^* = a_S e^{15(\varphi - \sigma)} - b_S e^{15(-\varphi - \sigma)} \quad (16)$$

The compliance of the stiffness adjuster is directly taken into consideration by calculating  $\varphi$ , since its position is directly influencing this calculation. The estimation of the parameters  $a_S, b_S$  is done with least square error optimization.

$$\mathbf{y} = M\mathbf{p} = M \begin{bmatrix} a_S \\ b_S \end{bmatrix}, \quad (17)$$

where  $M \in \mathfrak{R}^{N \times 2}$  is the data matrix consisting of the exponential parts,  $\mathbf{y} \in \mathfrak{R}^{N \times 1}$  the measurement vector containing joint torques, and  $\mathbf{p} \in \mathfrak{R}^{2 \times 1}$  the parameter vector. The calculated center line is denoted as  $\tau_{\text{mean}}$ . Obtaining  $\mathbf{p}$  is simply done by calculating the pseudoinverse of the observation matrix.

$$\mathbf{p} = (M^T M)^{-1} M^T \mathbf{y} \quad (18)$$

The results of this calculation are given in Tab. IV. The real stiffness coefficients vary up to  $\approx 35\%$  from the theoretical values. The asymmetry of the real values, which grows with increasing stiffness, can be explained by the slightly

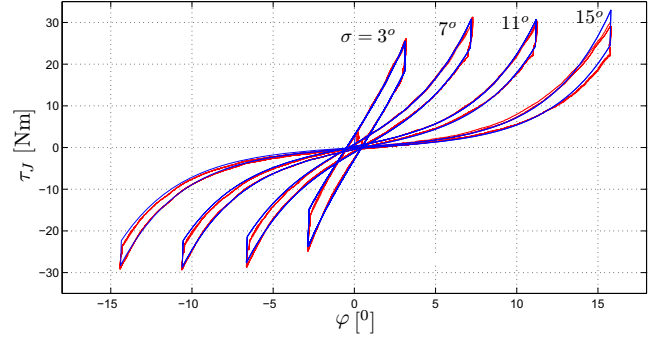


Fig. 9. Measured (red) and theoretical (blue) elastic response.

elastic behavior of the stiffness adjuster. However, please notice that the appealingly large value comes mainly from the fact  $\sigma$  is exponentially influencing the error. Furthermore, it becomes clear that the real friction torque  $\tau_F$  depends on  $\sigma$  and  $\varphi$ . No relation between velocity and friction could be observed, leading to neglecting viscous effects as already mentioned in Sec. IV-C, c.f. Fig. 7.

Figure 8 depicts the friction torque for different values of  $\sigma$ . The results indicate an exponential relation between  $\varphi$  and  $\tau_F$ . Taking a closer look leads to a linear relation between  $\tau_J$  and  $\tau_F$ . Therefore, it seems reasonable to model the friction as a sum of the torques resulting from the force input by each spring. This way the load free friction ( $\varphi = 0$ ) can be established and explained by the internal tension of the joint, increasing with growing  $\sigma$ . This leads to the following friction model.

$$\tau_F(\varphi) = a_F e^{15(\varphi - \sigma)} + b_F e^{15(-\varphi - \sigma)} \quad (19)$$

The coefficient estimation is again obtained by least-square error regression. The same structure as the one for the elastic joint torque can be obtained, except for the different sign for  $b_F$ . The numerical coefficients are listed in Tab. IV and a comparison of the measured and model is shown in Fig. 9.

## VI. PERFORMANCE INCREASE

In this section we report achieved from results formulating the maximization of link side velocity as an optimal control problem [16]. A paper fully describing the theory is currently under preparation. A theoretical analysis for the constant stiffness case is given in [15].

The model for the optimization is the one depicted in Fig. 7. Under the premise of achieving maximum deflection with one switching cycle, a limited velocity range results for the position motor. On the one hand, a minimum velocity for achieving the maximum deflection is needed and on the other side there exists a maximum velocity at which the constraints for maximum joint torque, motor torque and deflection can still be ensured. The theoretical and experimental results are depicted in Fig. 10, where the red marked points on the graphs were experimentally verified with the QA-Joint. It shows the relative velocity increase with respect to the motor velocity. The experimental values are indicated in green. The simulations were obtained with the parameters given in Tab. V.

If  $\epsilon = \frac{\dot{q}}{\theta_a}$  is considered as efficiency of the elastic mechanism it can be stated that  $\epsilon$  degrades with increasing motor velocity and increasing stiffness. For low stiffness it is necessary to drive with higher motor velocities to achieve the

Link inertia	$M$	0.523808 kgm <sup>2</sup>
Motor inertia	$B$	0.993374 kgm <sup>2</sup>
Proportional gain	$K_P$	25371
Differential gain	$K_D$	288
Maximum motor torque	$\tau_{m,max}$	160 Nm

TABLE V  
SYSTEM PARAMETERS

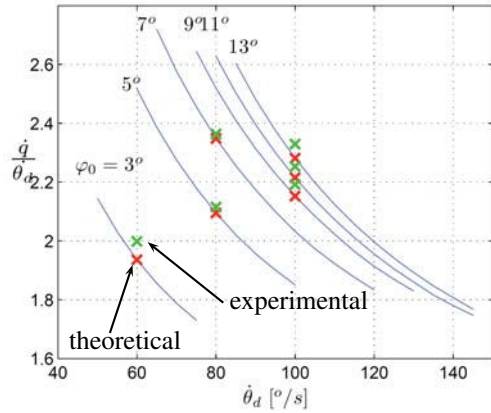


Fig. 10. Relative final link side velocity as a function of motor velocity.

maximum deflection. For the QA-Joint the largest efficiency  $\epsilon = 2.7$  can be obtained for  $\theta_d = 75$  °/s and  $\sigma = 7$  °.

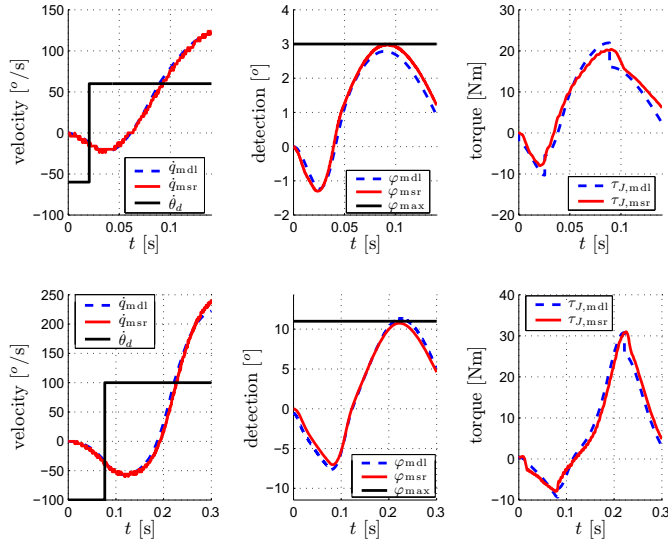


Fig. 11. Comparison of simulation and measurements for different stiffness presets. The upper upper shows the motion for  $\theta_d = 60$  °/s and  $\sigma = 3$  °. The lower row depicts the results for  $\theta_d = 100$  °/s,  $\sigma = 11$  °.

In Figure 11 the time evolution for measurements and simulation for  $\theta_d = 60$  °/s,  $\sigma = 3$  °, as well as  $\theta_d = 100$  °/s,  $\sigma = 11$  ° are shown. They confirm the consistency between theoretical prediction and experiment.

• **Link velocity (left):**

The trajectory of the link velocity shows very good consistency with the simulation. At final time it is approximately twice the motor velocity. The deviation in joint torque are almost not reflected in the velocity profile.

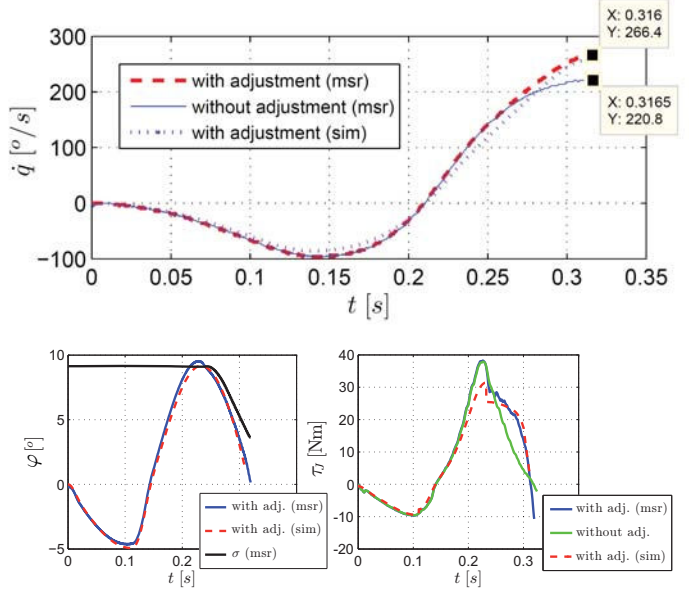


Fig. 12. Velocity with stiffness adjustment (upper). Deflection (lower left), and joint torque (lower right) with stiffness adjustment.

• **Deflection (middle):**

In contrast to the simulation, a slight exceedance of the deflection constraints  $\varphi_{max}$  can be observed. This is mainly due to the variance in the identified stiffness and friction parameters, calibration errors, and simplified assumptions for the friction model.

• **Joint torque (right):**

The principal time course of the joint torque confirms the joint model with respect to the identification of stiffness and friction. The discontinuities in the simulation are caused by the Coulomb friction model during change of direction.

For possible stiffness adjustment during the motion there are also some conclusions to be drawn. As shown in [16], *only* during the relaxation phase of a strike out trajectory further energy injection by stiffness adjustment is essential. Basically, the solution is the following desired stiffness trajectory in the relaxation phase.

$$\sigma_d = \varphi \quad (20)$$

For a moderate initial stiffness preset  $\sigma = 9$  ° the simulation and experiment are shown in Fig. 12. The achieved link velocity with stiffness adjustment is 266 °/s, which is approximately 20 % higher than without changing  $\sigma$ . Please note that the stiffness adjuster is assumed to show ideal behavior for the simulation.

From Figure 12 (lower left) it can be observed that adjusting the stiffness has slightly too little dynamics than is required to fulfill (20). Nonetheless, a significant velocity increase can be observed.  $\tau_J$  is comparably larger than for the constant case from the moment of adjustment on. Due to the slight exceedance of the theoretical deflection limits, the real joint torque is slightly higher and thus leads to larger link velocities than predicted by simulation.

In the next section we discuss a set of experiments for investigating the shock resistance of the joint and the performance of our control algorithms during such heavy disturbances.

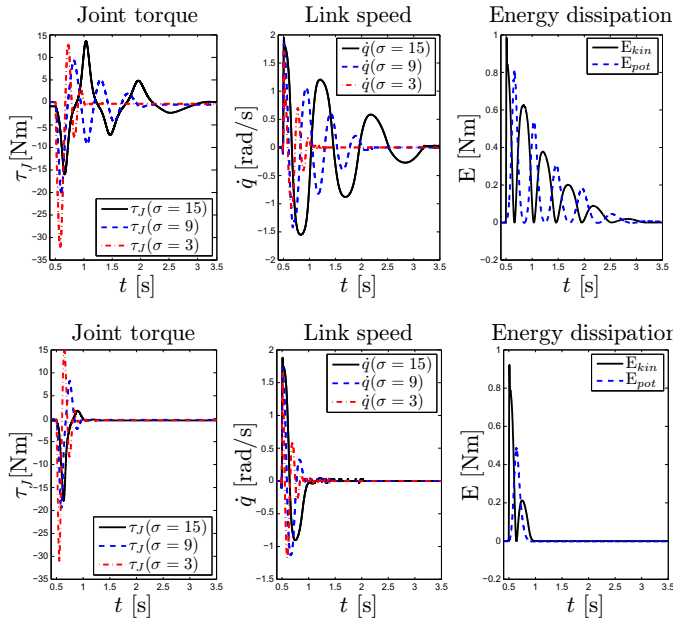


Fig. 13. Impact evolution without state feedback control (upper block) and with state feedback control (lower block). For readability the energies are only plotted for  $\sigma = 15$ .

## VII. JOINT PROTECTION AND CONTROL PERFORMANCE

In order to show the shock resistance and control performance of our joint design, we conducted impact drop tests with a rigid object acting on the link of the test joint. Figure 13 shows the behavior for three different stiffness preset values covering the entire range of the mechanism. The upper row depicts the measurements with the joint in position control and the lower row with full state feedback control [17] for vibration damping. The mass of the impactor is 4.2 kg and the impactor speed at the collision instant 1.07 m/s. The contact is rigid aluminum-brass, leading to very large collision forces of up to 5 kN, measured with a high bandwidth force sensor mounted on the impactor. The second column depicts the elastic joint torque, which oscillates strongly up to 3.5 s after the collision. The state feedback controller diminishes these oscillations effectively. Similar observations can be drawn for link speed and energy dissipation. Apart from the control performance even during these very high disturbance forces, the collision protection due to the elastic mechanism becomes apparent, when taking a closer look at the joint torque. Even for the rigid stiffness preset, the maximum nominal joint torque of 40 Nm is not reached despite the heavy impact. Furthermore, the large benefit of stiffness reduction can be observed. By setting the stiffness to the lowest preset, the impact joint torque can almost be halved.

## VIII. CONCLUSION

In this paper we introduced a classification of intrinsically compliant joint designs into *preload variable* and *transmission variable* types. Furthermore, we elaborated design considerations, which we believe to be important for building such joints: Well designed torque range, stiffness characteristics, and energy storage behavior are required for performance and robustness. As a consequence of these investigations a novel concept could be realized that intends to cover the identified desired properties. Its validity is

supported by several experiments, covering shock resistance, control performance, and elastic energy based speed up. A **video** attachment shows several experiments, outlining the performance of the joint.

## ACKNOWLEDGMENT

This work has been partially funded by the European Commission's Sixth Framework Programme as part of the project PHRIENDS under grant no. 045359 and VIACTORS under grant no. 231554. We would like to thank Sebastian Wolf and Markus Grebenstein for their excellent hardware support and the fruitful discussions about the concepts.

## REFERENCES

- [1] H. Iwata and S. Sugano, "Design of human symbiotic robot twenty-one bibtex," *IEEE Int. Conf. on Robotics and Automation (ICRA 2009), Kobe, Japan*, pp. 580–586, 2009.
- [2] D. Shin, I. Sardellitti, and O. Khatib, "Hybrid actuation approach for human-friendly robot design," in *IEEE Int. Conf. on Robotics and Automation (ICRA 2008), Pasadena, USA*, 2008, pp. 1741–1746.
- [3] A. Bicchi and G. Tonietti, "Fast and soft arm tactics: Dealing with the safety-performance trade-off in robot arms design and control," *IEEE Robotics and Automation Mag.*, vol. 11, pp. 22–33, 2004.
- [4] A. Albu-Schäffer, S. Haddadin, C. Ott, A. Stemmer, T. Wimböck, and G. Hirzinger, "The DLR Lightweight Robot Lightweight Design and Soft Robotics Control Concepts for Robots in Human Environments," *Industrial Robot Journal*, vol. 34, 2007.
- [5] M. Grebenstein and P. Smagt van der, "Antagonism for a highly anthropomorphic hand/arm system," *Advanced Robotics*, no. 22, pp. 39 – 55, 2008.
- [6] A. Albu-Schäffer, O. Eiberger, M. Grebenstein, S. Haddadin, C. Ott, T. Wimböck, S. Wolf, and G. Hirzinger, "Soft robotics: From torque feedback controlled lightweight robots to intrinsically compliant systems," *IEEE Robotics and Automation Mag.*, vol. 15, no. 3, pp. 20 – 30, 2008.
- [7] G. Pratt and M. Williamson, "Series elastics actuators," *IEEE/RSJ Int. Conf. on Intelligent Robots and Systems 1995 (IROS1995), Victoria, Canada*, pp. 399–406, 1995.
- [8] T. Morita and S. Sugano, "Development of one-dof robot arm equipped with mechanical impedance adjuster," *IEEE/RSJ Int. Conf. on Intelligent Robots and Systems (IROS2006), Washington, DC, USA*, p. 407, 1995.
- [9] R. Van Ham, B. Vanderborght, M. Van Damme, B. Verrelst, and D. Lefeber, "MACCEPA, the mechanically adjustable compliance and controllable equilibrium position actuator: Design and implementation in a biped robot," *Robotics and Autonomous Systems*, vol. 55, pp. 761–768, 2007.
- [10] C. Chou and B. Hannaford, "Measurement and modeling of mckibben pneumatic artificial muscles," *IEEE Transactions on Robotics and Automation*, no. 12, pp. 90–102, 1996.
- [11] S. Migliore, E. Brown, and S. DeWeerth, "Biologically inspired joint stiffness control," *IEEE Int. Conf. on Robotics and Automation (ICRA2005), Barcelona, Spain*, pp. 4508–4513, 2005.
- [12] J. W. Hurst, J. Chestnutt, and A. Rizzi, "An actuator with physically variable stiffness for highly dynamic legged locomotion," *IEEE Int. Conf. on Robotics and Automation (ICRA2004), Barcelona, Spain*, pp. 4662–4667, 2004.
- [13] S. Wolf and G. Hirzinger, "A new variable stiffness design: Matching requirements of the next robot generation," *IEEE Int. Conf. on Robotics and Automation (ICRA 2008), Pasadena, USA*, pp. 1741–1746, 2008.
- [14] R. Schiavi, G. Grioli, S. Sen, and A. Bicchi, "VSA-II: a novel prototype of variable stiffness actuator for safe and performing robots interacting with humans," *IEEE Int. Conf. on Robotics and Automation (ICRA2008), Pasadena, USA*, pp. 2171–2176, 2008.
- [15] S. Haddadin, T. Laue, U. Frese, S. Wolf, A. Albu-Schäffer, and G. Hirzinger, "Kick it like a safe robot: Requirements for 2050," *Robotics and Autonomous Systems: Special Issue on Humanoid Soccer Robots*, vol. 57, pp. 761–775, 2008.
- [16] M. Weis, "Optimalsteuerungskonzepte für Robotergelenke mit einstellbarer passiver Steifigkeit," Master's thesis, German Aerospace Center (DLR) & TH Karlsruhe, 6 2009.
- [17] A. Albu-Schäffer, S. Wolf, O. Eiberger, S. Haddadin, F. Petit, and M. Chalon, "Dynamic modeling and control of variable stiffness actuators," in *IEEE Int. Conf. on Robotics and Automation (ICRA 2010), Anchorage, Alaska*, 2010.